Journal of Southeast University (English Edition) Vol. 31, No. 4, pp. 479 - 488 Dec. 2015 ISSN 1003—7985

CFD simulation of ammonia-based CO_2 absorption in a spray column

Zhao Jie Jin Baosheng Xu Yin

(Key Laboratory of Energy Thermal Conversion and Control of Ministry of Education, Southeast University, Nanjing 210096, China)

Abstract: A comprehensive computational fluid dynamics (CFD) model is developed based on the gas-liquid two-phase hydrodynamics, gas-liquid mass-transfer theory and chemical reaction kinetics, and the ammonia-based CO_2 absorption in a spray column is numerically studied. The Euler-Lagrange model is applied to describe the behavior of gas-liquid two-phase flow and heat transfer. The dual-film theory and related correlations are adopted to model the gas-liquid mass transfer and chemical absorption process. The volatilization model of multi-component droplet is utilized to account for ammonia slippage. The effect of operation parameters on CO_2 removal efficiency is numerically studied. The results show a good agreement with the previous experimental data, proving the validity of the proposed model. The profile studies of gas-phase velocity and CO_2 concentration suggest that the flow field has a significant impact on the CO_2 concentration field. Also, the local CO_2 absorption rate is influenced by both local turbulence and the local liquid-gas ratio. Furthermore, the velocity field of gas phase is optimized by the method of adjusting the orifice plate, and the results show that the CO_2 removal efficiency is improved by approximately 4%.

Key words: CO_2 absorption; spray column; computational fluid dynamics(CFD); aqueous ammonia

doi: 10.3969/j.issn.1003-7985.2015.04.009

The segregation and storage of CO_2 discharge from thermal power plants has been a concern among human beings due to global warming and deteriorating ecosystems. Although its natural volatilization still hinders its development, ammonia-based CO_2 capture has been considered as a potential approach among various CO_2 removal methods due to its high CO_2 removal efficiency, large absorption capacity, weak tendency to degradation, and low cost[1]. Recently, three types of reactors have been proposed for ammonia-based CO_2 capture, namely, tray columns, packed columns, and spray columns. Compared with the two other reactors, the spray column is more feasible for a large mass-transfer area and resistant to the block of the reactor caused by the precipitation of NH_4HCO_3[2].

Numerous studies on CO_2 capture in a spray column have been undertaken. Kuntz et al.[2] studied the mass-transfer performance of a spray column, and compared it to that of a packed column. The results demonstrate a great potential in using the spray column in the CO_2 capture application. Lim et al.[3] experimentally studied the performance of CO_2 capture with a single nozzle, and reported the correlation between the capture efficiency and the operation parameters. Niu et al.[4] compared three kinds of absorbents in the same spray column, and the results show that the CO_2 removal efficiency by aqueous ammonia is higher than that by both NaOH and MEA. Javed et al.[5] found that the imparting swirl in the gas flow can enhance the overall mass transfer coefficient up to around 49%.

Compared with the experiment, simulation studies based on CFD software package have the advantages of convenience and low-cost, especially visualization for three-dimensional distribution of operation parameters. Many investigations of CO_2 capture using numerical simulation methods have been conducted. However, most of them focused on the bubble column and packed column[6-9]. Numerical simulation studies on CO_2 capture in the spray column is rarely available. Furthermore, some of them ignored the CO_2 absorption process and emphasized the gas-liquid flow field in the spray column[10]. However, in order to optimize the operation parameters, it is essential to obtain the CO_2 concentration distribution. Thus, incorporating the CO_2 reactive absorption submodel into the overall model is very important. Besides, the study of the correlation between the flow field and CO_2 concentration field is rather significant for optimizing the flow field and improving CO_2 removal efficiency. Therefore, there is urgent need for further study in this area to examine the feasibility of ammonia-based CO_2 absorption in a spray column.

In this paper, a comprehensive CFD model incorporated with mass transfer, chemical reaction and two-phase flow is developed to describe ammonia-based CO_2 absorption in a spray column. Comparing the simulation results and the experimental data found in the previous literature, the effects of different operation parameters on CO_2 removal efficiency are studied. Ammonia slippage is also predicted numerically using the volatilization model of a multi-component droplet. After analyzing the law of flow

Received 2015-05-04.

Biographies: Zhao Jie (1991—), female, graduate; Jin Baosheng (corresponding author), male, professor, bsjin@seu.edu.cn.

Foundation item: The National Natural Science Foundation of China (No. 51276038).

Citation: Zhao Jie, Jin Baosheng, Xu Yin. CFD simulation of ammonia-based CO_2 absorption in a spray column[J]. Journal of Southeast University (English Edition), 2015, 31(4): 479 - 488. [doi: 10.3969/j.issn.1003-7985.2015.04.009]

field and CO_2 concentration field, a strategy for flow field optimization is adopted and CO_2 removal efficiency is improved.

1 Model Description

1.1 Physical model

The sketch of a spray column used in this work is shown in Fig. 1(a). Flue gas flows in the spray column from the bottom inlet, and goes up through the spray layers. Absorbent aqueous ammonia is sprayed from atomizers on the spray layers, makes contact with flue gas counter-current, and absorbs CO_2 in the meantime. The treated gas flows upwards and goes through demister where water vapor is eliminated. Aqueous ammonia which has absorbed CO_2 (rich solution) falls down to the column bottom. To simplify the model, the computational region is limited to a rich solution level and the effect of the rich solution on the flow field of flue gas is not considered. Assume that the demister zone has little effect on the flow field of flue gas and mass transfer. In order to eliminate the error caused by the difference in structure size, the spray column in Zeng's experiment[11] was taken as the simulation object(see Fig. 1(b)). The detailed flue gas and spray absorbent parameters are listed in Tab. 1.

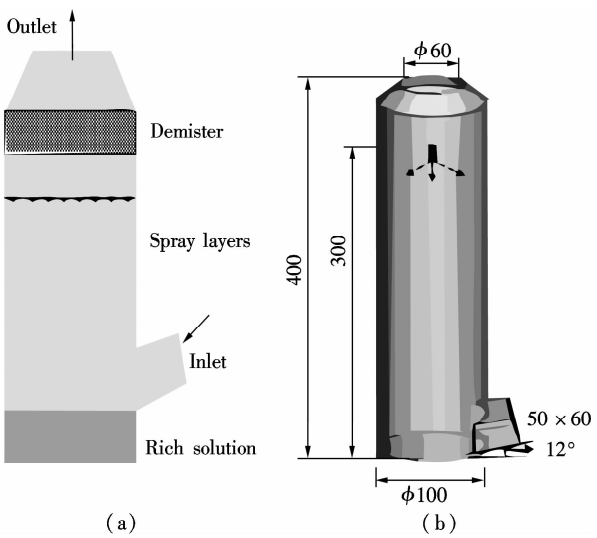

Fig. 1 Structure sketch of spray column. (a) Schematic sketch; (b) Physical mode(unit: mm)

Tab. 1 Modeling parameters of spray column

Parameter	Value
Flue gas temperature/℃	50
Inlet velocity/(m · s^{-1})	0.056 to 0.155
Flue gas composition	CO_2, N_2
w_{CO_2}/%	15
Aqueous ammonia temperature/℃	15 to 35
$w_{NH_3 \cdot H_2O}$/%	2 to 8
Spray velocity/(m · s^{-1})	5
Spray angle/(°)	60
Flow rate of atomizer/(g · s^{-1})	2.16 to 6.40
Diameter of droplets/μm	30 to 40

Prior to performing the numerical simulations, several assumptions were made: 1) Flue gas is an incompressible Newtonian fluid and is treated as an ideal gas; 2) Liquid droplets are treated as a rigid sphere, and their diameters follow the Rosin-Rammber distribution; 3) Since droplet diameters are very uniform, collision between droplets is ignored[12]. In this study, the Weber number is far less than 1, the crack of droplets can be ignored[13-14]. Additionally, according to Refs. [15-16], the coalescence of droplets is also ignored; 4) The variations of flue gas velocity and droplet drag coefficient, resulting from droplet evaporation, droplet deformation and mass-transfer process, are not considered; 5) Once liquid droplets make contact with the wall, they will flow down along the wall and not affect the gas phase.

When carrying out the three-dimensional modeling and hypermesh, the whole column was divided into several different bodies to generate structured hexahedral meshes to improve the calculation accuracy. For the gas phase, the velocity inlet and pressure outlet were set to be the boundary conditions. Liquid phase was set as the escape. The second-order upwind was adopted as discretization schemes for conservative equations. SIMPLEC algorithms were applied to calculate the pressure-velocity coupled steady flow.

1.2 Hydrodynamical model

The fluid dynamics inside a spray column is typically a two-phase flow consisting of continuous flue gas and a large number of dispersed liquid droplets. In this paper, since the total volume ratio of dispersed liquid is far less than 10%, the E-L model is applied to simulate the behavior of the two-phase flow and heat transfer. The main advantage of using the Lagrangian framework for dispersed phase flow is that the particle-level phenomena can be modeled rigorously. Besides, droplet size distribution and droplet-wall interaction can be easily taken into account. The gas phase is simulated in the Eulerian frame. The standard k-ε model and the standard wall function are adopted to describe the fully developed turbulence region and turbulence region near the wall, respectively. The universal equation for continuity, momentum, turbulence kinetic energy, dissipation rate, energy and concentration equation can be expressed as[17]

$$\frac{\partial(\rho\phi)}{\partial t}+\frac{\partial(\rho u\phi)}{\partial t}+\frac{\partial(\rho v\phi)}{\partial t}+\frac{\partial(\rho w\phi)}{\partial t}=\frac{\partial}{\partial t}\left(\Gamma\frac{\partial\phi}{\partial x}\right)+\frac{\partial}{\partial t}\left(\Gamma\frac{\partial\phi}{\partial y}\right)+\frac{\partial}{\partial t}\left(\Gamma\frac{\partial\phi}{\partial z}\right)+S \quad (1)$$

where ρ is the density of the gas phase, kg/m^3; ϕ defines universal dependent variable; Γ represents the diffusion coefficient for different equations; S is the source term for different equations. The expressions of ϕ, Γ, S are presented in Tab. 2.

Tab. 2 Parameters listed in universal equation

Conservative equation	ϕ	Γ	S
Mass	1	0	S_m
Momentum-x	u	$\mu_{eff}=\mu+\mu_t$	$-\frac{\partial P}{\partial x}+\frac{\partial}{\partial x}\left(\mu_{eff}\frac{\partial u}{\partial x}\right)+\frac{\partial}{\partial y}\left(\mu_{eff}\frac{\partial u}{\partial x}\right)+\frac{\partial}{\partial z}\left(\mu_{eff}\frac{\partial u}{\partial x}\right)+S_u$
Momentum-y	v	$\mu_{eff}=\mu+\mu_t$	$-\frac{\partial P}{\partial y}+\frac{\partial}{\partial x}\left(\mu_{eff}\frac{\partial u}{\partial y}\right)+\frac{\partial}{\partial y}\left(\mu_{eff}\frac{\partial u}{\partial y}\right)+\frac{\partial}{\partial z}\left(\mu_{eff}\frac{\partial u}{\partial y}\right)+S_v$
Momentum-z	w	$\mu_{eff}=\mu+\mu_t$	$-\frac{\partial P}{\partial z}+\frac{\partial}{\partial x}\left(\mu_{eff}\frac{\partial u}{\partial z}\right)+\frac{\partial}{\partial y}\left(\mu_{eff}\frac{\partial u}{\partial z}\right)+\frac{\partial}{\partial z}\left(\mu_{eff}\frac{\partial u}{\partial z}\right)+S_w$
Turbulence kinetic energy	κ	$\mu+\frac{\mu_t}{\sigma_\kappa}$	$G_\kappa+\rho\varepsilon$
Dissipation rate	ε	$\mu+\frac{\mu_t}{\sigma_\varepsilon}$	$\frac{\varepsilon}{\kappa}(C_{1\varepsilon}G_\kappa-C_{2\varepsilon}\rho\varepsilon)$
Energy	T	$\frac{\mu}{Pr}+\frac{\mu_t}{\sigma_T}$	S_T
Concentration	C_i	$\rho\left(D+\frac{Dt}{\sigma'_{\varepsilon c}}\right)$	S_c

Spray liquids are described by the discrete particle model, and the random walk model is adopted to describe the influence of turbulence on the motion of liquid droplets. In gas-liquid flow regions with a low density ratio, only the steady-state drag force and the gravity force contribute to the linear momentum variation of particles. Other forces such as thermophoretic force, brownian, and saffman lift force etc. are ignored[18].

The dispersed phase particle trajectory is solved by the integration of particle force equation. The particle force equation is[13]

$$\frac{du_p}{dt}=F_D(u-u_p)+\frac{g_x(\rho_p-\rho)}{\rho_p} \tag{2}$$

where the first term on the right side of Eq. (2) is the drag of unit mass for particle, $F_D=\frac{18\mu}{\rho_p d_p^2}\frac{C_D Re}{24}$, where $Re=\frac{\rho d_p|u_p-u|}{\mu}$ $C_D=a_1+\frac{a_2}{Re}+\frac{a_3}{Re}$; the second term is the particle gravity. u is the continuous phase velocity, m/s; u_p is the particle phase velocity, m/s; μ is the viscosity of continuous phase, Pa · s; ρ is the density of continuous phase, kg/m^3; ρ_p is the density of the particle, kg/m^3; d_p is the particle diameter, m.

When considering the gas-liquid mass transfer, the effect of gas absorption on the continuous phase is described in the source terms (S_m, S_u, S_T, S_c) of different conservative equations.

1.3 CO_2 absorption model and validation

1.3.1 CO_2 absorption process in the spray column

Generally, the CO_2 absorption rate is expressed as[19]

$$\frac{dc_{CO_2}}{dt}=-N_{CO_2}\alpha \tag{3}$$

where c_{CO_2} is the Mole concentration of CO_2 in the liquid phase, mol/m^3; t is the absorption time, s; α is the effective gas-liquid interfacial area in unit volume, m^2/m^3; N_{CO_2} is the overall mass-transfer flux, mol/(m^2 · s).

As is well known, the process of ammonia-based CO_2 absorption is an inter-phase mass-transfer process. With the diameters of liquid droplets as small as tens of micrometers, the internal circulation can be ignored. Thus, according to the dual-film theory, for steady CO_2 absorption process, the overall mass-transfer flux equation is

$$N_{CO_2}=K_G(p_{CO_2}-p_{CO_2,i}) \tag{4}$$

where K_G is the overall mass-transfer coefficient in the gas phase, mol/(m^2 · s · Pa); p_{CO_2} is the partial pressure of CO_2 in the gas phase, Pa; $p_{CO_2,i}$ is the equilibrium partial pressure of CO_2 at the interface, Pa.

For rapid chemical reactions, $p_{CO_2,i}$ is far less than the partial pressure of CO_2 in the gas phase p_{CO_2}, so $p_{CO_2,i}$ is approximately 0[11,20]. The overall mass-transfer coefficient K_G in the gas phase is expressed as

$$\frac{1}{K_G}=\frac{1}{k_G}+\frac{H_{CO_2}}{\beta k_L} \tag{5}$$

where k_G is the mass-transfer coefficient in the gas phase, mol/(m^2 · s · Pa); k_L is the mass-transfer coefficient in the liquid phase without chemical reaction, m/s; β is the chemical reaction enhancement factor; H_{CO_2} is Henry's constant of CO_2, (Pa · m^3)/mol.

k_G is obtained by the Frossling equation as[19,21]

$$Sh=\frac{k_G d}{D_{CO_2}}=2+0.55Re^{0.5}Sc^{0.333} \tag{6}$$

where Re is the Reynolds number; Sh and Sc are the Sherwood number and the Schmidt number, respectively.

$$Re=\frac{d|u_G-u_L|\rho_G}{\mu_G};\quad Sc=\frac{\mu_G}{\rho_G D_{CO_2}}$$

$$D_{CO_2}=\frac{9.86\times10^{-9}T^{1.75}(1/M_{N_2}+1/M_{CO_2})^{0.5}}{1\times10^{-6}P(v_{CO_2}^{1/3}+v_{N_2}^{1/3})}$$

where d is the diameter of liquid droplet, m; u_G and u_L are the velocities of flue gas and liquid droplet, m/s; ρ_G and μ_G are the density and viscosity of flue gas, kg/m^3 and Pa · s, respectively; D_{CO_2} is the diffusion coefficient of CO_2 in the gas phase, m^2/s; M_{N_2} and M_{CO_2} are the mole mass of N_2 and CO_2, kg/kmol; v_{N2} and v_{CO_2} are the molecular volume of N_2 and CO_2, cm^3 · mol.

k_L is obtained by the following Sherwood relationship[6]:

$$Sh = \frac{k_L d}{D^L_{CO_2}} = 2 + 0.15 Re_d^{0.89} Sc^{0.7} \quad (7)$$

where $D^L_{CO_2}$ is the diffusion coefficient of CO_2 in aqueous ammonia, m/s, estimated from the viscosity of aqueous ammonia using a modified Stokes-Einstein equation[22]:

$$D^L_{CO_2} = D^{H_2O}_{CO_2}\left(\frac{\mu_{H_2O}}{\mu_{NH_3\text{-}H_2O}}\right)^{0.8} \quad (8)$$

$$D^{H_2O}_{CO_2} = 2.35 \times 10^{-6} \exp\left(\frac{-2\,119}{T}\right) \quad (9)$$

where $D^{H_2O}_{CO_2}$ is the diffusion coefficient of CO_2 in water, m/s; μ_{H_2O} and $\mu_{NH_3\text{-}H_2O}$ are the viscosity of water and aqueous ammonia, respectively, Pa · s.

For lower ammonia concentration ($<10\%$) of aqueous ammonia, ammonia concentration has little effect on Henry's law constant. So, we can use Henry's law constant of CO_2 in water to estimate Henry's law constant of CO_2 in aqueous ammonia[23]. Zeng[11] used the following correlation:

$$H_{CO_2} = 2.824\,9 \times 10^6 \exp\left(\frac{-2\,044}{T}\right) \quad (10)$$

β is defined as the ratio of chemical absorption rate to physical absorption rate. Despite several complex reaction equations accounting for CO_2 absorption in aqueous ammonia[24-25], the researchers considered it a pseudo-first-order irreversible reaction. In the case that the absorption occurs in the so-called pseudo-first-order regime ($3 < Ha \leqslant \beta_i$)[22], β equals the Hatta number.

$$\beta = Ha = \frac{\sqrt{k_{ov} D^L_{CO_2}}}{k_L} \quad (11)$$

where is β_i is the instant chemical reaction enhancement, Ha is the Hatta number; k_{ov} is the pseudo-first-order reaction rate selected from the experimental results by Zeng[11].

For liquid droplets generated by pressure-swirl atomizer, Liu et al.[26-27] proposed a method to calculate the overall surface area by the correlation related to the Sauter mean diameter.

$$A_d = \frac{Q}{0.036\ We^{-0.396\,43} Re_d^{0.136\,33} d_0} \quad (12)$$

where A_d is the overall surface area of all the droplets, m^2; Q is the total flow rate of spray liquid, m^3/s^2; We and Re_d are the Weber number and Reynolds number, respectively.

$$We = \frac{\rho_G (u_G + u_L)^2 d}{\sigma}, \quad Re_d = \frac{\rho_L (u_L + u_G) d}{\mu_L}$$

where ρ_L and μ_L are the density and viscosity of flue gas, respectively, kg/m^3 and Pa · s; σ is the surface tension of spray liquid, N/m.

Therefore, α can be estimated as

$$\alpha = \frac{A_d}{V} \quad (13)$$

where V is the total volume of the spray column, m^3.

Then, we can obtain the CO_2 absorption rate in the form of mole concentration.

$$\frac{dc_{CO_2}}{dt} = -N_{CO_2}\alpha = -K_G \alpha p_{CO_2} \quad (14)$$

$K_G\ \alpha$ is defined as the volumetric overall mass-transfer coefficient, mol · Pa/(m^3 · s).

Therefore, the source term of mass conservative equation, S_m, is expressed as

$$S_m = -N_{CO_2}\alpha M_{CO_2} = -K_G \alpha p_{CO_2} M_{CO_2} \quad (15)$$

and the source term of CO_2 concentration equation, S_c, is expressed as

$$S_c = -N_{CO_2}\alpha M_{CO_2} = -K_G \alpha p_{CO_2} M_{CO_2} \quad (16)$$

The above source terms accounting for CO_2 absorption process are programmed as a user-defined function (UDF) file and loaded into Fluent 6.3 software to complete the numerical simulations.

1.3.2 Validation of CO_2 absorption model

Fig. 2 shows the comparison of the volumetric overall mass-transfer coefficient from mathematical model data ($K_G\alpha'$) and Zeng's experimental results ($K_G\alpha$). As can be seen, the relative error is within the trust-region of 10%, suggesting that the CO_2 absorption model is appropriate for ammonia-based CO_2 absorption in spray columns. We note that the calculated values from the mathematical model are a little lower than that of experimental result. The discrepancy may come from calculation of the averaged effective gas-liquid interfacial area in the unit volume. In fact, the local effective gas-liquid interfacial area in the unit volume varies in different regions in a spray column. There can be certain error to utilize an averaged one. Moreover, limitation of correlation for the mass-transfer coefficient k_L, k_G and β may give rise to a

certain deviation. Besides, the variation of two-phase hydrodynamics resulting from the absorption process is ignored, which directly affects the gas-liquid two-phase flow, blend and mass transfer. Seen from the modeling of CO_2 absorption, α appears in each of the conservation equations of mass, momentum, and concentration. Hence, it is pointed out that accurate modeling of the local effective interfacial area in unit volume is the first step to simulate and predict the mass transfer performance of a spray column[6].

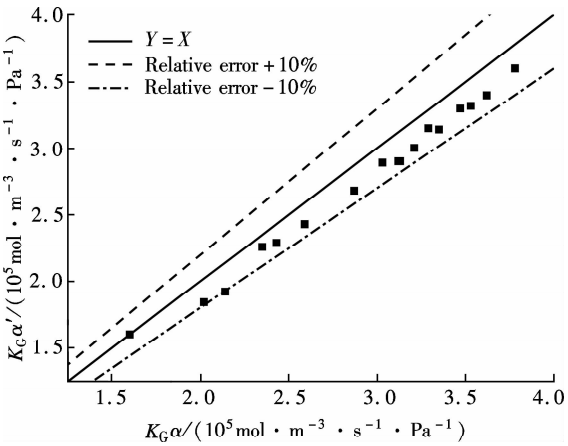

Fig. 2 Comparison of the volumetric overall mass-transfer coefficient

2 Results and Discussion

In this paper, the CO_2 removal efficiency is defined as

$$\eta = \frac{C_{out} - C_{in}}{C_{in}} \times 100\% \qquad (17)$$

where C_{out} is the averaged mass concentration of CO_2 of the outlet and C_{in} is the averaged mass concentration of CO_2 of the inlet.

2.1 Analysis of CO_2 removal efficiency and ammonia slippage

2.1.1 The effect of ammonia concentration

Fig. 3 is a typical plot of CO_2 removal efficiency and ammonia slippage as a function of ammonia concentration in the spray column under the following conditions: the inlet flow of flue gas is 20 L/min; CO_2 concentration is 15%; aqueous ammonia flow rate is 8 L/h and temperature is 20 ℃. Ammonia concentration has a great impact on CO_2 removal efficiency and ammonia slippage, and the simulation result is consistent with the experimental data. As the ammonia concentration increases from 2% to 8%, the CO_2 removal efficiency doubles. The increase of aqueous ammonia concentration increases the free ammonia concentration at the gas-liquid interface, which greatly promotes chemical equilibrium to move forwards and decreases mass-transfer resistance in the liquid phase. As a result, it clearly accelerates the chemical absorption rate and increases CO_2 removal efficiency. However, it is important to note that the free ammonia of high concentration at the gas-liquid interface can easily spread to the gas phase, leading to secondary pollution. As seen from Fig. 3, when aqueous ammonia is at a low concentration ($\leqslant$ 4%), the amount of ammonia slippage is less than 0.25%. While aqueous ammonia is at a high concentration ($>$6%), the amount of ammonia slippage increases exponentially. When the ammonia concentration increases from 6% to 8%, ammonia slippage increases by about 0.9%. In actual application, the ammonia concentration should not be too high in order to avoid a large amount of ammonia slippage.

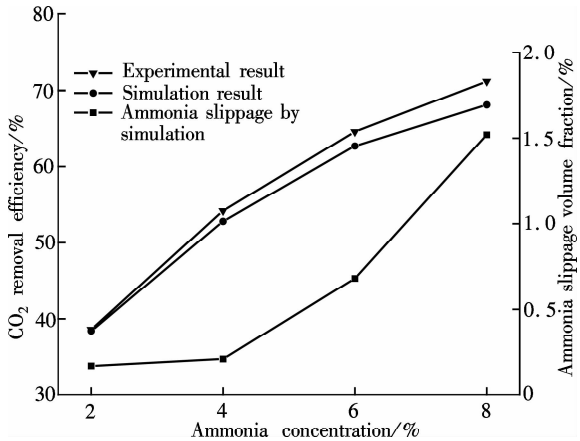

Fig. 3 Profile of the effect of ammonia concentration

2.1.2 The effect of aqueous ammonia flow rate

The variations of CO_2 removal efficiency and ammonia slippage with the ammonia aqueous flow rate in the spray column are shown in Fig. 4 under the following conditions: the inlet flue gas flow rate is 20 L/min; CO_2 concentration is 15%; the ammonia concentration of ammonia aqueous is 6% and temperature is 20 ℃. In the range of allowable error, the simulation result is in good agreement with the experimental data. As the aqueous ammonia flow rate increases from 8 to 20 L/h, CO_2 removal efficiency increases by around 9%. The observed little increase in the CO_2 removal efficiency may be attributed to the restriction of other operating parameters. The CO_2 absorption rate is notably dependent upon the flow rate of aqueous ammonia. It is also dependent upon the retention time of the flue gas. The aqueous ammonia flow rate promotes CO_2 removal efficiency in two ways. First, the increase of aqueous ammonia flow rate leads to the reduction in the size of spray droplets and the increase in the number of droplets, which can apparently increase α. Secondly, owing to the finite chemical reaction rate, the increase in the aqueous ammonia flow rate may increase the concentration of free ammonia at the gas-liquid interface, which is a driving force for chemical absorption. Thus, for aqueous ammonia with high concentration, the effect of the increase of free ammonia concentration at the

gas-liquid interface becomes insignificant, leaving α to be the primary factor that increases the CO_2 removal efficiency. On the other hand, the increase of free ammonia concentration at the gas-liquid interface leads to the increase of ammonia slippage. When the aqueous ammonia flow rate increases from 12 to 20 L/h, ammonia slippage increases by approximately 0.4%. From the comparison of Fig. 4 and Fig. 3, it is concluded that ammonia slippage growth resulting from the increase of the aqueous ammonia flow rate is not so dramatic as that resulting from the increase of ammonia concentration. A suggestion for industrial application is that low concentration and appropriately excessive aqueous ammonia should be used to maintain high CO_2 removal efficiency and low ammonia slippage.

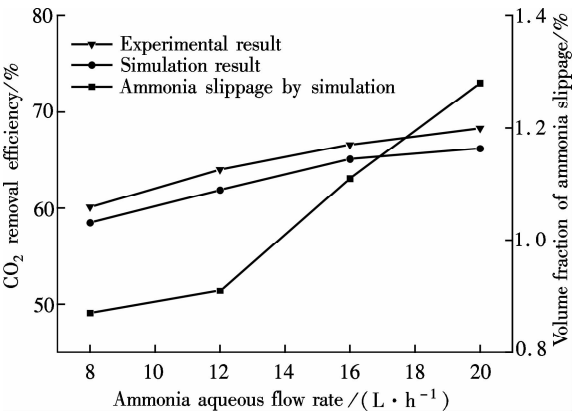

Fig. 4 Profile of the effect of aqueous ammonia flow rate

2.1.3 The effect of the flue gas flow rate

Fig. 5 illustrates the variations of CO_2 removal efficiency and ammonia slippage with the flue gas flow rate under the following conditions: the ammonia aqueous flow rate is 16 L/min; CO_2 concentration is 15%; the ammonia concentration is 6% and the temperature is 20 ℃. As is seen, the simulation curve has the same trend as the experimental data, with a large error at a high flow rate of flue gas. With the flow rate of flue gas increasing from 10 to 28 L/min, the CO_2 removal efficiency reduces by nearly 30%. In a specific spray column, the increase of flue gas flow rate means an increase in the flue gas velocity. To some degree, the increase of flue gas velocity enhances gas-phase turbulence, which decreases gas-phase mass transfer resistance and promotes gas-liquid mass transfer. However, the increase of flue gas velocity greatly shortens gas-liquid two-phase contact time, which weakens the gas-liquid two-phase blend and mass transfer. The ultimate outcome is the reduction of CO_2 removal efficiency. On the other hand, the negative impact on gas-liquid mass transfer reduces CO_2 absorption flux, which substantially increases pH at the gas-liquid interface and causes ammonia volatilization into gas phase[28]. When the flue gas flow rate increases from 10 to 20 L/min, ammonia slippage increases by about 0.1%. While the flue gas flow rate increases from 20 to 28 L/min, ammonia slippage increases by about 0.3%. Thus, in actual application, a spray column should operate under the condition of the designed standard flue gas amount to avoid massive ammonia slippage.

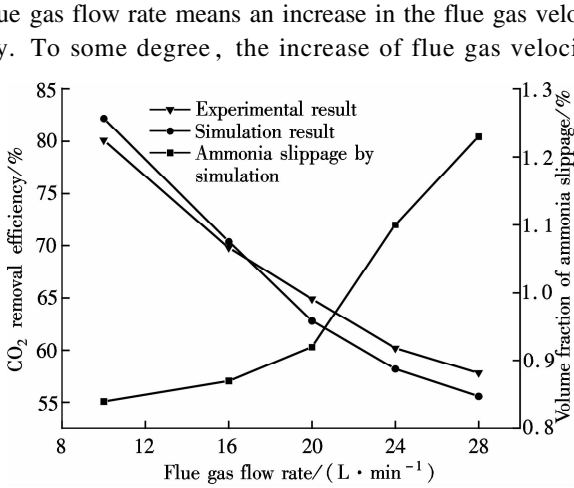

Fig. 5 Profile of the effect of flue gas flow rate

Comparing simulated and experimental CO_2 removal efficiency, it is concluded that the comprehensive CFD model is appropriate for predicting ammonia-based CO_2 absorption in the spray column. It should be noted that the simulation value is a little smaller than that of experimental result. The following reasons are responsible for the discrepancy. First, the calculational error of the volumetric overall mass-transfer coefficient directly causes the error of CO_2 removal efficiency. Secondly, the local reflux of flue gas in the spray column is ignored in the numerical simulation, which lengthens gas-liquid contact time and strengthens gas-liquid mass transfer.

It is notable that, in actual application, the ammonia that is emitted into the atmosphere is much less than that of the numerical simulation. On the one hand, the volatilization model of the multi-component droplet is not accurate for the electrolyte solution with chemical reactions. On the other hand, the water wash apparatus connected to the outlet of spray column can tremendously reduce ammonia emissions into the atmosphere[29]. It is found that both pressurized operation and water scrubbers can reduce ammonia slippage[8]. Besides, adopting the modified solution by adding additives (PZ, ionic liquids, Cu^{2+} etc.) to aqueous ammonia can effectively decrease ammonia slippage[30].

2.2 Parameters distribution field and optimization

From the above result, the maximum CO_2 removal efficiency is around 75% when the flue gas flow rate is 20 L/min. In order to improve CO_2 removal efficiency, further study on the correlation of velocity field and CO_2 absorption is shown in this section.

2.2.1 Parameters distribution field

Two-phase parameters distribution are presented in Fig. 6 to Fig. 10, which are simulated under the conditions that the artificial flue gas flow rate is 20 L/min; the inlet CO_2 concentration is 15%; the ammonia concentration is 4% and the aqueous ammonia flow is 8 L/h.

Fig. 6 shows the three-dimensional distribution of the gas phase velocity magnitude. As seen from Fig. 6(a) that after entering the inlet, except for a little flue gas circling on the rich solution level, most of the flue gas impinges against the left wall, forming a high velocity zone along the left wall between the elevation of about 50 and 120 mm. The impingement causes the flow direction of flue gas to turn to the right side. This can be clearly observed in the velocity vector distribution(see Fig. 7(a)). While the flue gas changes flow direction, a swirl zone with a low velocity is produced above the inlet, as shown in Fig. 7(b). Then, with the flue gas flowing upwards, a high velocity zone along the right wall between elevation of about 150 and 250 mm occurs. As seen from Fig. 6(b), the velocity distribution on the longitudinal section $x=0$ is symmetric. Except for a high velocity zone and a low velocity zone affected by gas entrance, the flow field is relatively uniform. Fig. 6(c) shows the radical variation of velocity magnitude at different elevations ($z=50$, 100, 150, 200, 250, 300, 350, 400 mm). Fig. 7(c) shows the droplet trajectory distribution. Droplets with longer residence time exist in the bottom region of the column.

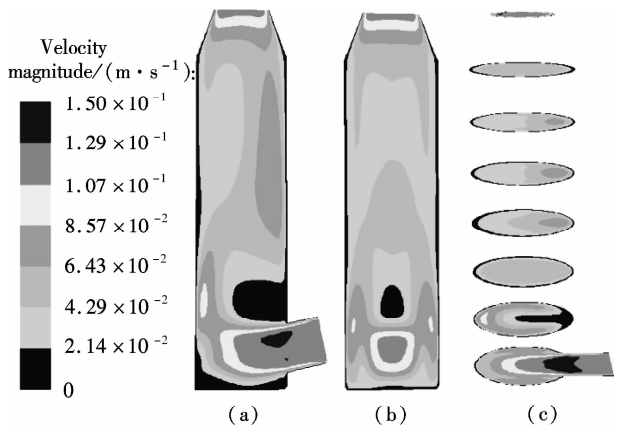

Fig. 6 Velocity magnitude distribution on longitudinal sections and horizontal sections. (a) $x=0$; (b) $y=0$; (c) Elevations

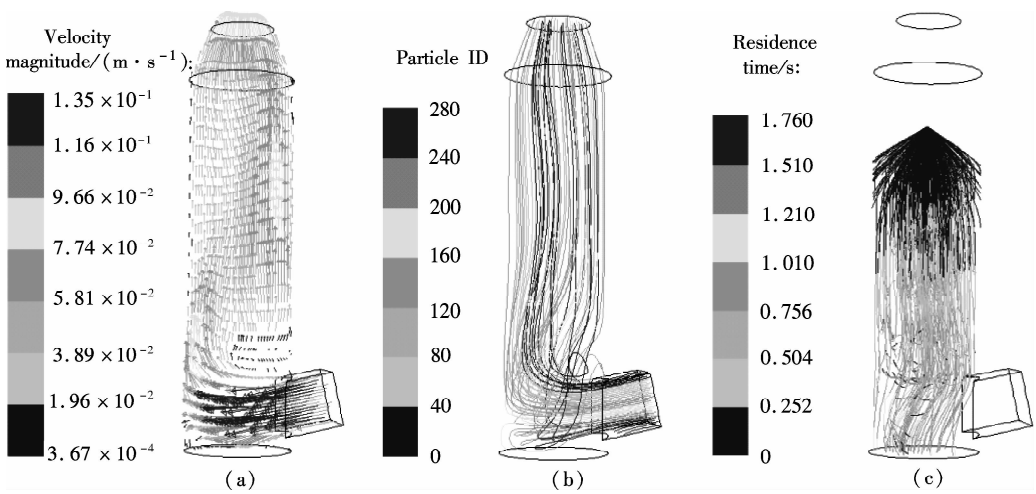

Fig. 7 Parameter distribution. (a) Velocity vector distribution; (b) Gas phase pathlines; (c) Particle distribution

The three-dimensional distribution of CO_2 concentration in the spray column is shown in Fig. 8. Seen from the color of longitudinal sections (Figs. 8(a) and (b)), the CO_2 concentration value decreases gradually with the flue gas flowing up. However, many contour lines of CO_2 concentration are not level, indicating that the radical distribution of CO_2 concentration is not equal at the same horizontal plane. Similar to velocity distribution, CO_2 concentration distribution on longitudinal section $x=0$ is symmetric. Horizontal sections at different elevations are shown in Fig. 8(c), including $z=50$, 100, 150, 200, 250, 300, 350, 400 mm. As can be seen, a local radical difference of CO_2 concentration generally exists. This is caused by a radical deviation of gas velocity. As is known, the increase of local gas velocity enhances gas phase turbulence and strengthens gas-liquid mass transfer, thus leading to the decrease in the local liquid-gas ratio. Thus, the influence of local gas velocity on CO_2 concentration is the result of the combination of local turbulence and local liquid-gas ratio. This is in agreement with Ref. [19].

Fig. 9 and Fig. 10 show the velocity magnitude and

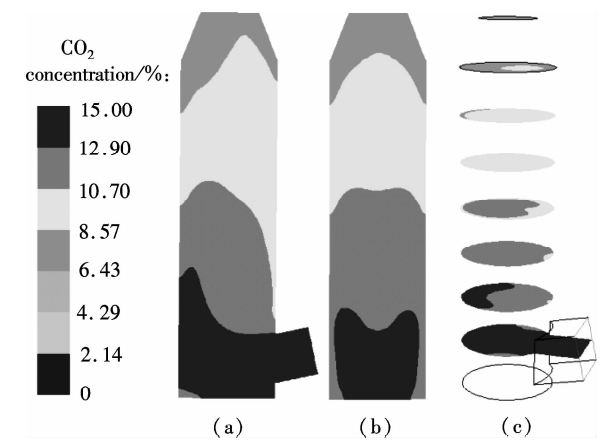

Fig. 8 CO_2 concentration on longitudinal sections and horizontal sections. (a) $x=0$; (b) $y=0$; (c) Elevations

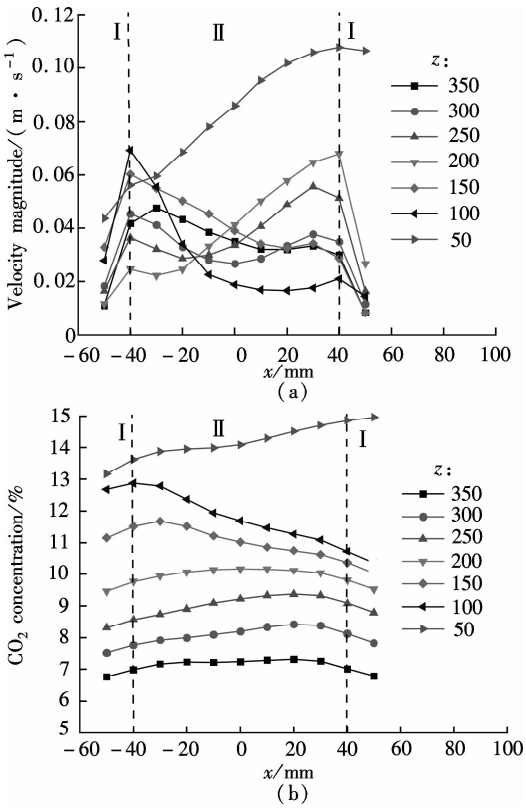

Fig. 9 Velocity magnitude and CO_2 concentration distribution on longitudinal section $y = 0$. (a) Velocity magnitude distribution; (b) CO_2 concentration distribution

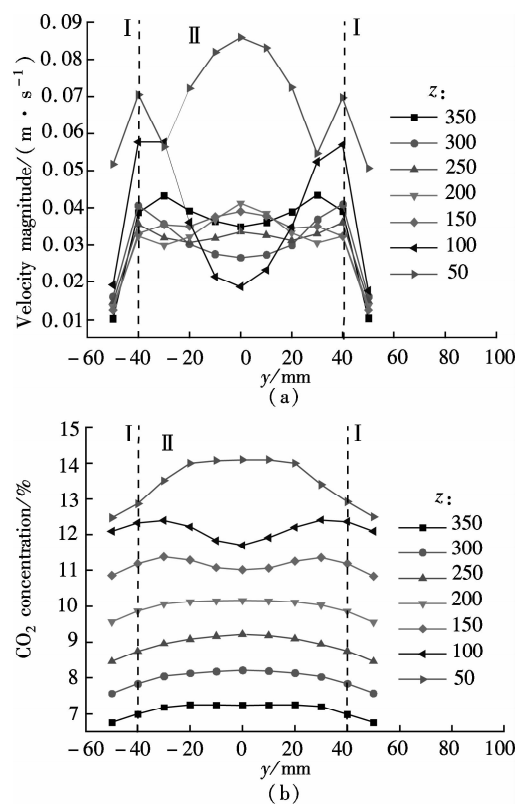

Fig. 10 Velocity magnitude and CO_2 concentration distribution on longitudinal section $x = 0$. (a) Velocity magnitude distribution; (b) CO_2 concentration distribution

CO_2 concentration distribution on longitudinal sections. The figures can be divided into two regions: region Ⅰ and region Ⅱ. Region Ⅰ is the region near the wall. In region Ⅰ, when the area is far from the wall, the gas velocity and CO_2 concentration are high. This is because the resistance for gas flow is large in the area near the wall. Region Ⅱ is the region where the gas flow field significantly affects CO_2 concentration distribution.

The influence of local gas velocity on the radical distribution of CO_2 concentration is shown in Fig. 9 and Fig. 10. From Figs. 9(a) and (b), it can be seen that when z = 100, 150 and 250 mm, the CO_2 concentration is low in the area where the gas velocity is high. This means that the increase in the local gas velocity can decrease the local CO_2 absorption rate, indicating that the liquid-gas ratio is the main factor for CO_2 absorption on these elevations. However, when z = 200 and 350 mm, the CO_2 concentration remains even in the area where the gas velocity is high. This can be explained by the contribution made by local turbulence and the liquid-gas ratio which may be counteracted. A similar phenomenon can be found in Figs. 10(a) and (b). The radical distribution of CO_2 concentration becomes more uniform when the column elevation increases.

2.2.2 Optimized parameters distribution field

From the analysis above, the high velocity zone in the local region weakens the local CO_2 absorption rate to some degree. Due to its capability of effectively organizing gas flow, the orifice plate is arranged in the simulation model(z = 80 mm) to optimize the parameters distribution field under the same operation conditions.

Fig. 11 and Fig. 12 show the three-dimensional distribution of gas phase velocity magnitude and CO_2 concentration after arranging the orifice plate. Comparing Fig. 6 and Fig. 11, it is clear that after arranging the orifice plate, the swirl zone above the inlet and two high velocity zones disappear. The impingement phenomenon no longer occurs and the gas phase velocity in the spray column becomes more uniform. The orifice plate has a positive

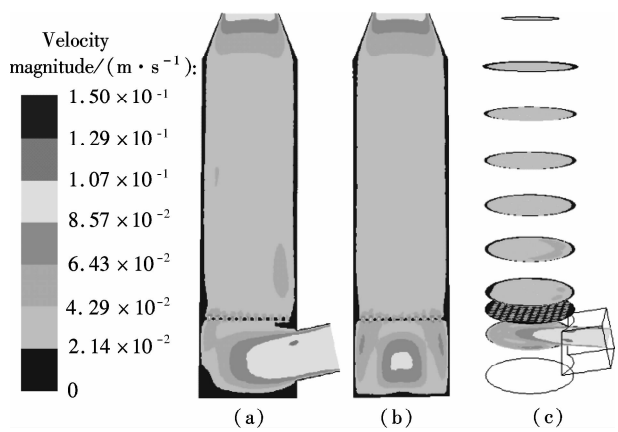

Fig. 11 Velocity magnitude distribution on longitudinal sections and horizontal sections. (a) $x = 0$; (b) $y = 0$; (c) Elevations

effect on organizing gas flow and preventing reflux. Comparing Fig. 8 and Fig. 12, it is clear that at the same elevation, the contour lines of CO_2 concentration become greater even after arranging the orifice plate, indicating that the radical distribution of CO_2 concentration become more uniform. This is due to the reduction of the radical deviation of gas velocity.

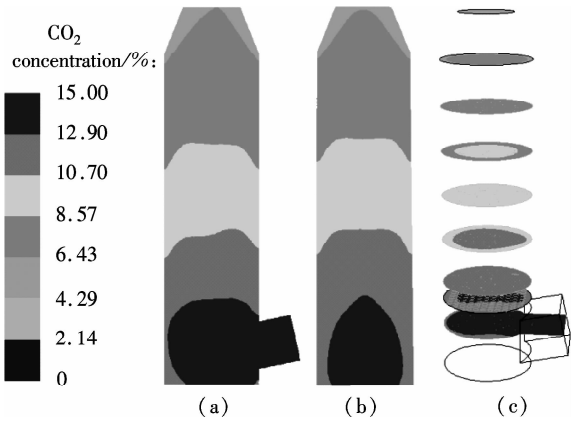

Fig. 12 CO_2 concentration on longitudinal sections and horizontal sections. (a) $x=0$; (b) $y=0$; (c) Elevations

Fig. 13 is the plot of the variation of CO_2 removal efficiency with spray column elevation. The CO_2 concentration at different horizontal planes is the averaged value by surface integration. As can be seen, CO_2 removal efficiency increases rapidly below the spray layer (300 mm) due to the high absorbent droplets concentration and large gas-liquid mass-transfer area. While CO_2 removal efficiency increases slightly above the spray layer since there is few absorbent droplets except for those entrained. The slope of these curves decreases with the increase of elevation. This means that CO_2 removal amount within the unit height column decreases with the increase of elevation. This can be explained, with the flue gas flowing up, CO_2 is absorbed gradually, and the reduction of CO_2 partial pressure leads to the decrease of CO_2 absorption rate. Additionally, when the orifice plate is arranged, CO_2 removal efficiency on each horizontal plane is improved a little, and the ultimate CO_2 removal efficiency is improved by around 4%.

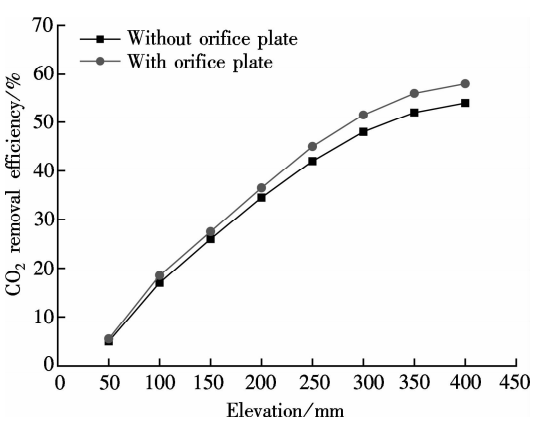

Fig. 13 Variation of CO_2 removal efficiency with elevation

3 Conclusion

1) The increase of aqueous ammonia flow rate and ammonia concentration can both promote CO_2 removal efficiency, but ammonia slippage growth resulting from the increase in aqueous ammonia flow rate is not so dramatic as that resulting from the increase of ammonia concentration. The increase in flue gas flow rate can decrease CO_2 removal efficiency and increase ammonia slippage.

2) Local gas velocity has a significant influence on the radical CO_2 concentration distribution. The influence of local gas velocity on local CO_2 absorption rate is the result of the combination of local turbulence and local liquid-gas ratio.

3) By arranging an orifice plate on the physical model, the high gas velocity zone and large vortex are eliminated and the ultimate CO_2 removal efficiency is improved by about 4%.

References

[1] Yeh A C, Bai H L. Comparison of ammonia and monoethanolamine solvents to reduce CO2 greenhouse gas emissions[J]. *Science of the Total Environment*, 1999, **228**(2/3):121 - 133.

[2] Kuntz J, Aroonwilas A. Performance of spray column for CO_2 capture application [J]. *Industry & Engineering Chemistry Research*, 2007, **47**(1):145 - 153.

[3] Lim Y, Choi M, Han K, et al. Performance characteristics of CO_2 capture using aqueous ammonia in a single-nozzle spray tower[J]. *Industry & Engineering Chemistry Research*, 2013, **52**(43):15131 - 15137.

[4] Niu Zhenqi, Guo Yincheng, Lin Wenyi. Carbon dioxide removal efficiencies by fine sprays of MEA, NaOH and aqueous ammonia solutions[J]. *Journal of Tsignhua University*, 2010, **50**(7):1130 - 1140. (in Chinese)

[5] Javed K H, Mahmud T, Purba E. The CO_2 capture performance of a high-intensity vortex spray scrubber [J]. *Chemical Engineering Journal*, 2010, **162**(2): 448 - 456.

[6] Zhang D S, Deen N G, Kuipers G A M. Euler-Euler modeling of flow, mass transfer, and chemical reaction in a bubble column[J]. *Industry & Engineering Chemistry Research*, 2009, **48**(1): 47 - 57.

[7] Zhang D S. Eulerian modeling of reactive gas-liquid flow in a bubble column [D]. Enschede, The Netherlands: University of Twente, 2007.

[8] Yu Hai, Morgan S, Allport A, et al. Results from trialling aqueous NH_3 based post-combustion capture in a pilot plant Munmorah power station: absorption[J]. *Chemical Engineering Research and Design*, 2011, **89**(8): 1204 - 1215.

[9] Liu Guobiao. Computational transport and its application to mass transfer and reaction processes in packed-beds [D]. Tianjin: School of Chemical Engineering, University of Tianjin, 2006. (in Chinese)

[10] Lu Tongchang. Experimental research and CFD simulation of ammonia absorption of CO_2 from flue gas [D].

Baoding: School of Energy, Power and Mechanical Engineering, North China Electrical Power University, 2013. (in Chinese)
[11] Zeng Qing. The experimental investigation on CO_2 absorption by aqueous ammonia[D]. Beijing: School of Aerospace Engineering, TsingHua University, 2011. (in Chinese)
[12] Zhu Jie, Wu Zhenyuan, Ye S, et al. Drop size distribution and specific surface area in spray tower[J]. *Journal of Chemical Industry and Engineering*, 2014, **65**(12): 4710-4715. (in Chinese)
[13] Cai Bin, Li Lei, Wang Zhaolin. Numerical analysis of liquid droplet breakup in airflow[J]. *Journal of Engineering Thermophysics*, 2003, **24**(4): 613-616. (in Chinese)
[14] Du Zhanbo, Mao Jingru, Sun Bi. Measurements of droplet sizes at mid-hight of stationary turbine blades and analysis of the critical weber number[J]. *Journal of Power Engineering*, 2005, **25**(5): 643-684. (in Chinese)
[15] Li Tongming. Coalescence between small bubbles or droplets[J]. *Journal of Chemical Industry and Engineering*, 1994, **45**(1): 38-44. (in Chinese)
[16] Li Tongming, Zhao Liyan. The influence of interfacial rheological property on coalescence process of small droplet[J]. *Acta Physico-Chimica Sinica*, 1996, **12**(8): 708-714. (in Chinese)
[17] Yu Guocong, Yuan Xigang. *Computational mass transfer introduction for chemical engineering process*[M]. Tianjin: Tianjin University Press, 2011. (in Chinese)
[18] Fluent Inc. Fluent user's guide[EB/OL]. (2006-09)[2015-05-15]. http://wenku.baidu.com/link?url=MU4BlrL5d_b-uHKVD41mdubXvw94p9FQ22UXE_EQStKH5piDiYVwDgCPcT4Ib43S5D5rMRVAdy-XsC2VE9RYpidwEi_fd8jSzaoDya4eX9a.
[19] Zhong Yi, Gao Xiang, Wang Huiting, et al. The performance optimization of the wet flue gas desulfurization system based on CFD[J]. *Proceedings of the CSEE*, 2008, **28**(32): 18-23. (in Chinese)
[20] de Montigny D, Tontiwachwuthikul P, Chakma A. Comparing the absorption performance of packed columns and membrane contactors[J]. *Industry & Engineering Chemistry Research*, 2005, **44**(15): 5726-5732.
[21] Warych J, Szymanowski M. Model of the wet limestone flue gas desulfurization process for cost optimization[J]. *Industry & Engineering Chemistry Research*, 2001, **40**(12): 2597-2605.
[22] Derks P W J, Versteeg G F. Kinetics of absorption of carbon dioxide in aqueous ammonia solutions[J]. *Energy Procedia*, 2009, **1**(1): 1139-1146.
[23] Liu Jinzhao, Wang Shujuan, Qi Guojie, et al. Kinetics and mass transfer of carbon dioxide absorption into aqueous ammonia[J]. *Energy Procedia*, 2011(4): 525-532.
[24] Liu Jinzhao, Wang Shujuan, Zhao Bo, et al. Absorption of carbon dioxide in aqueous ammonia[J]. *Energy Procedia*, 2009, **1**(1): 933-940.
[25] Bai H L, Yeh A C. Removal of CO_2 greenhouse gas by ammonia scrubbing[J]. *Industry & Engineering Chemistry Research*, 1997, **36**(6): 2490-2493.
[26] Liu Nailing, Zhang Xu. Experimental study of atomization characteristic of pressure spiral nozzle[J]. *Journal of Experiments for Fluid Mechanics*, 2006, **20**(3): 8-12. (in Chinese)
[27] Chen Hongyu, Liu Guorong. The theoretical study of a novel water-spraying desulfurization by aqueous ammonia [J]. *General Machinery*, 2007(4): 23-26. (in Chinese)
[28] Budzianowski W M. CO_2 reactive absorption from flue gases into aqueous ammonia solutions: the NH_3 slippage effects[J]. *Environment Protection Engineering*, 2011, **37**(4): 5-19.
[29] Li Liqing, Zhang Chun, Huang Guijie, et al. A multicomponent droplet model in simulating mass transfer of the ammonia-based spray process[J]. *Proceedings of the CSEE*, 2014, **34**(32): 5741-5749. (in Chinese)
[30] Liu Xi. Experimental research on effects of additives to the ammonia-based CO_2 capture process[D]. Nanjing: School of Energy and Environment, Southeast University, 2014. (in Chinese)

喷淋塔氨法脱碳的 CFD 模拟

赵 杰 金保昇 徐 寅

(东南大学能源热转换及其过程测控教育部重点实验室, 南京 210096)

摘要:基于气液两相流体力学、气液传质理论和化学反应动力学,建立了综合的 CFD 模型,并对喷淋塔内氨水脱碳进行了数值研究. 采用欧拉-拉格朗日模型描述了气液两相流动特性和传热情况. 根据双膜理论及相关的关联式,对气液传质和化学吸收过程进行了建模. 采用多组分液滴的挥发模型模拟氨水的挥发过程. 通过数值模拟研究了运行参数对 CO_2 脱除效率的影响,并与现有的文献结果进行对比,验证了模型的正确性. 气相速度和 CO_2 浓度的分析表明,流场对 CO_2 的浓度场有着重要的影响. CO_2 的局部吸收速率受局部湍流和局部液气比的共同影响. 此外,采用加装孔板的方法对气相流场进行了优化,结果表明 CO_2 脱除效率提高了约 4%.

关键词:CO_2 吸收;喷淋塔;计算流体力学;氨水

中图分类号:TK09